

Effect of Plasma-Enhanced Low-Temperature Chemistry on Deflagration-to-Detonation Transition in a Microchannel

Sandia National Laboratory, Livermore, California 94550 Xingqian Mao,[‡] Zhiyu Shi,[§] Andrey Starikovskiy,[¶] and Yiguang Ju** Princeton University, Princeton, New Jersey 08544

Christopher Kliewer ††

Sandia National Laboratory, Livermore, California 94550

https://doi.org/10.2514/1.J062966

This study examines low-temperature chemistry (LTC) enhancement by nanosecond dielectric barrier discharge (ns-DBD) plasma on a dimethyl ether (DME)/oxygen (O_2) /argon (Ar) premixture for deflagration-to-detonation transition (DDT) in a microchannel. It is found that non-equilibrium plasma generates active species and kinetically accelerates LTC of DME and DDT. In situ laser diagnostics and computational modeling examine the influence of the ns-DBDs on the LTC of DME and DDT using formaldehyde (CH $_2$ O) laser-induced fluorescence (LIF) and high-speed imaging. Firstly, high-speed imaging in combination with LIF is used to trace the presence of LTC throughout the flame front propagation and DDT. Then, competition between plasma-enhanced LTC of ignition and reduced heat release rate of combustion due to plasma-assisted partial fuel oxidation is studied with LIF. Observations of plasma-enhanced LTC effects on DDT are interpreted with the aid of detailed kinetic simulations. The results show that an appropriate number of ns-DBDs enhances LTC of DME and increases CH $_2$ O formation and low-temperature ignition, accelerating DDT. Moreover, it is found that, with many ns-DBDs, CH $_2$ O concentration decreases, indicating that excessive discharges may accelerate fuel oxidation in the premixture, reducing heat release and weakening shock–ignition coupling, inhibiting DDT.

I. Introduction

MPROVING the energy conversion efficiency of power generation through combustion is an important step in reducing carbon emissions. Existing gas turbine engines use a constant-pressure Brayton cycle, which limits their thermal efficiency. Advanced pressure-gain power generation using a constant-volume cycle, such as a rotating detonation engine (RDE), has the potential to increase efficiency by up to 30% [1]. However, detonation stability remains a big challenge for airbreathing or lean-burn RDEs [2,3]. Plasma-assisted combustion provides a great opportunity to accelerate deflagration-to-detonation transition (DDT) as well as promises stronger shock—flame coupling to increase detonation stability, which would ultimately make such advanced engines feasible [4,5]. However, few studies have been carried out to understand the effect of plasma-assisted combustion

Presented as Paper 2023-2057 at the AIAA SciTech Forum 2023, National Harbor, MD, January 23–27, 2023; received 3 March 2023; revision received 1 July 2023; accepted for publication 16 July 2023; published online 25 August 2023. Copyright © 2023 by the American Institute of Aeronautics and Astronautics, Inc. Under the copyright claimed herein, the U.S. Government has a royalty-free license to exercise all rights for Governmental purposes. All other rights are reserved by the copyright owner. All requests for copying and permission to reprint should be submitted to CCC at www.copyright.com; employ the eISSN 1533-385X to initiate your request. See also AIAA Rights and Permissions www.aiaa.org/randp.

*Ph.D. Candidate, Department of Mechanical and Aerospace Engineering.
Student Member AIAA.

[†]Postdoctoral Appointee, Combustion Research Facility; currently Research Scientist, Lawrence Livermore National Laboratory. Member AIAA.

*Postdoctoral Research Associate, Department of Mechanical and Aerospace Engineering; xingqian@princeton.edu (Corresponding Author).

§Ph.D. Candidate, Department of Mechanical and Aerospace Engineering. Student Member AIAA.

[¶]Research Specialist, Department of Mechanical and Aerospace Engineering. Senior Member AIAA.

**Robert Porter Patterson Professor, Department of Mechanical and Aerospace Engineering. Associate Fellow AIAA.

††Distinguished Member of Technical Staff, Combustion Research Facility.

on DDT for use in applied engines, especially for fuels involving low-temperature chemistry (LTC) [6–8].

Our recent studies have examined the influence of pulsed nanosecond discharges on the premixture and on the resultant DDT onset time and distance through the use of high-speed imaging [9]. A highspeed camera was used to trace the time histories of flame front position and velocity and to identify the dynamics and onset of DDT. The results showed that nanosecond discharge can nonlinearly affect the onset time and distance of DDT. It was shown that a small number of high-voltage pulses before ignition result in reduced DDT onset time and distance by 60 and 40%, respectively, when compared to the results without pre-excitation by nanosecond discharges. The results also showed that an increase in the number of pulses results in an extended DDT onset time and distance of 224 and 94%, respectively, and excessive partial oxidation. Time history of the deflagration wave speed of dimethyl ether (DME) and the analysis of ignition timescale suggest that low-temperature ignition may play a role for DME near the isobaric choking condition of the burned gas. These experiments demonstrated the ability of non-equilibrium plasma to alter the chemistry of DME/O₂/Ar premixtures in order to control DDT for applications in advanced propulsion engines. However, two questions remain. The first is whether the LTC of DME is indeed enhanced by nanosecond discharge in DDT. The second is determining the cause of the observed increase of DDT onset time with a large number of high-voltage pulses, aside from the previously observed partial fuel oxidation. To answer these two questions, in situ high-speed measurements of formaldehyde, CH2O, a critical indicator of LTC of DME oxidation, in plasma-assisted DDT processes with different number of high-voltage nanosecond pulses are needed.

The goal of this study is to conduct *in situ* laser diagnostics and computational modeling to examine the influence of the nanosecond discharge on the LTC of DME and DDT. At first, experiments both without and with a uniform nanosecond dielectric barrier discharge (ns-DBD) plasma applied across a 1-mm-tall, 5-mm-wide, \sim 60-cm-long combustion channel filled with DME/O₂/Ar premixture at an equivalence ratio near the lean limit ($\Phi = 0.7$) are conducted. The

coupled laser-induced fluorescence (LIF) and high-speed imaging techniques are used to trace the CH_2O species distributions temporally and spatially during deflagration. Then, the competition between the plasma-enhanced kinetic effect on ignition and the reduced heat release rate in the combustion wave front due to the excessive partial fuel oxidation is studied experimentally and numerically.

II. Experimental and Numerical Methods

The microscale channel for plasma-assisted DDT study used in these experiments is a uniform ns-DBD plasma discharge applied across a channel with 1 mm in height, 5 mm in width, and \sim 60 cm in length filled with a dimethyl ether/oxygen/argon (0.132 DME/0.568 O₂/0.3 Ar) mixture. The experimental setup is nearly identical to that detailed in [9] with the exception that the channel width has been increased from 4 to 5 mm to allow for laser access through the ends of the channel. The channel is filled and vented through additional ports at either end. The channel construction and the experimental setup are highlighted in Figs. 1a and 1b.

In the first series of experiments, the combustion experiments, a single burst of 500 pulses with a pulse width of 200 ns is generated by a DC high-voltage supply and pulser (Eagle Harbor, NSP-120-20-N), controlled by a signal generator (Fig. 1c). Each nanosecond pulse is 10 kV, 200 ns and the pulse rate within the singular burst is 10 kHz. This moderately high number of pulses is used to slightly delay the DDT onset compared to a case with a smaller number of pulses, and to extend the propagation region associated with the fuel's LTC as identified in [9]. In the second series of experiments, the plasma experiments, a trigger initiates a sequence of 10 kV, 10 kHz, 200 ns pulses in bursts of varying quantities at a burst rate of 20 Hz (Fig. 1d).

A. High-Speed Imaging

A Phantom v1610 high-speed complementary metal oxide semiconductor (CMOS) camera recording at 200 kHz is used to image the chemiluminescence emitted from the propagating flame-front and trace its position and velocity, as well as to locate the region of interest. Figure 2 shows the characteristic positions (a) and velocity profiles (b) for cases with and without plasma. Similar to the previous work, [9], it is observed that plasma discharge accelerates DDT onset, the point of which is highlighted in the figures. It seemingly does so by leveraging the suspected LTC velocity spike. This and other observations of the detonation onset process are discussed specifically to this experiment in [9], and more generally in [10]. As such, they will not be repeated here. This region of this peak becomes our region of interest for LIF experiments and the experimental LIF moments are indicated on both plots. The timing and field of view of the CMOS are then adjusted accordingly to capture the flame front in this stage of propagation.

B. Laser-Induced Fluorescence

Formaldehyde generated by plasma-enhanced LTC of DME in the experiments is excited by the third harmonic of an Nd:YAG at 355 nm. The beam enters the end of the channel, focused by a 3 m lens, and runs the 600 mm length of the 1×5 mm cross-section channel allowing for excitation throughout the entire length of the channel. The beam energy is 2–3 mJ within the test section. An Andor iStar intensified charge coupled device (ICCD) camera equipped with two Semrock FF01-CH2O-25 filters captures the CH₂O LIF image. The intensifier gate is set to 20 ns.

In the plasma-enhanced LTC and DDT experiments, the LIF is captured in the regions of interest identified through high-speed imaging. These instants for LIF signals are indicated in Fig. 2. In the plasma experiments, the ICCD camera captures the CH₂O LIF

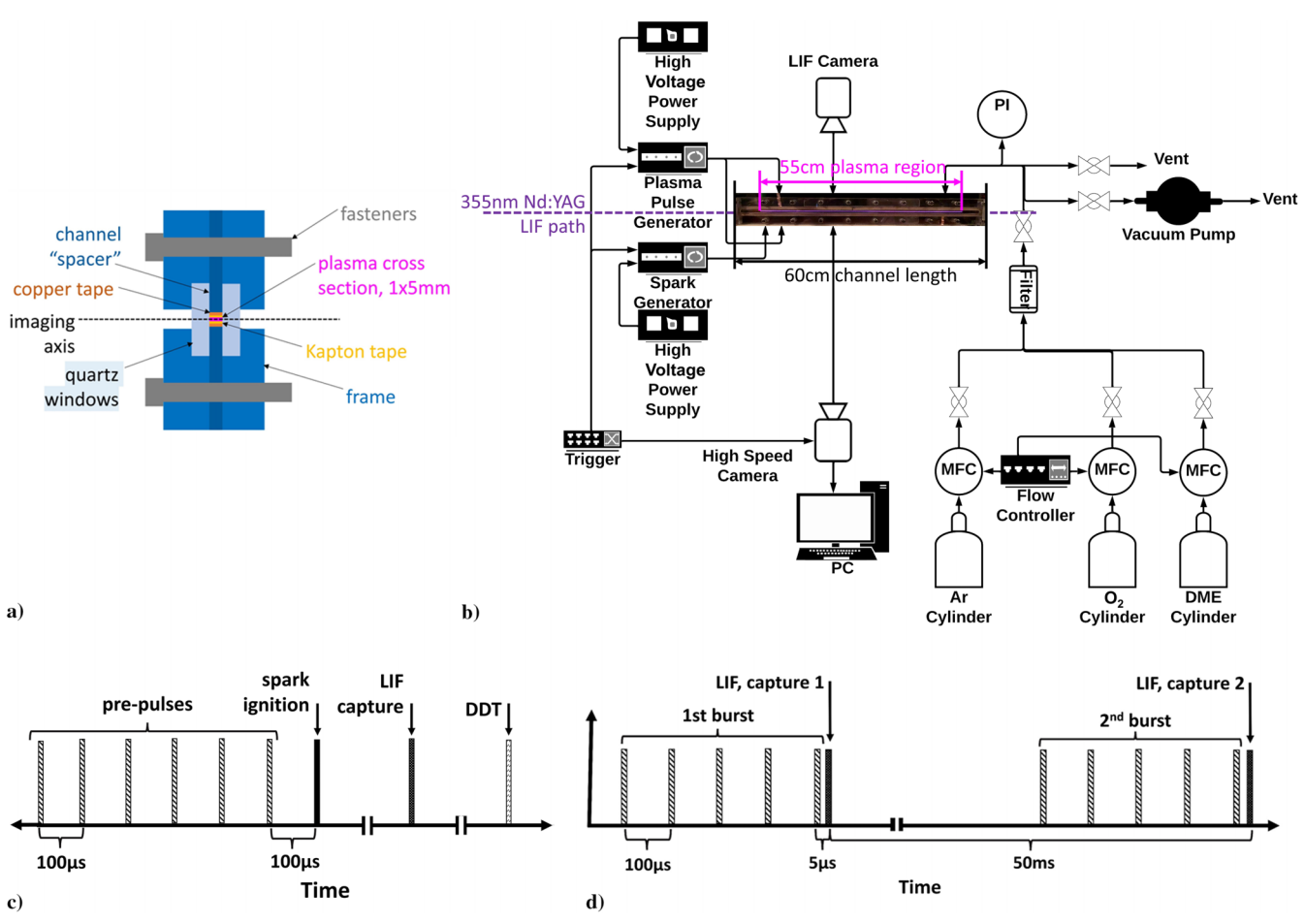


Fig. 1 a) Cross section of plasma channel detailing construction. b) Schematic overview of experimental setup. c) Timing diagram for combustion experiments. d) Timing diagram for experiments without combustion (an example case of the 5-pulse burst condition is shown).

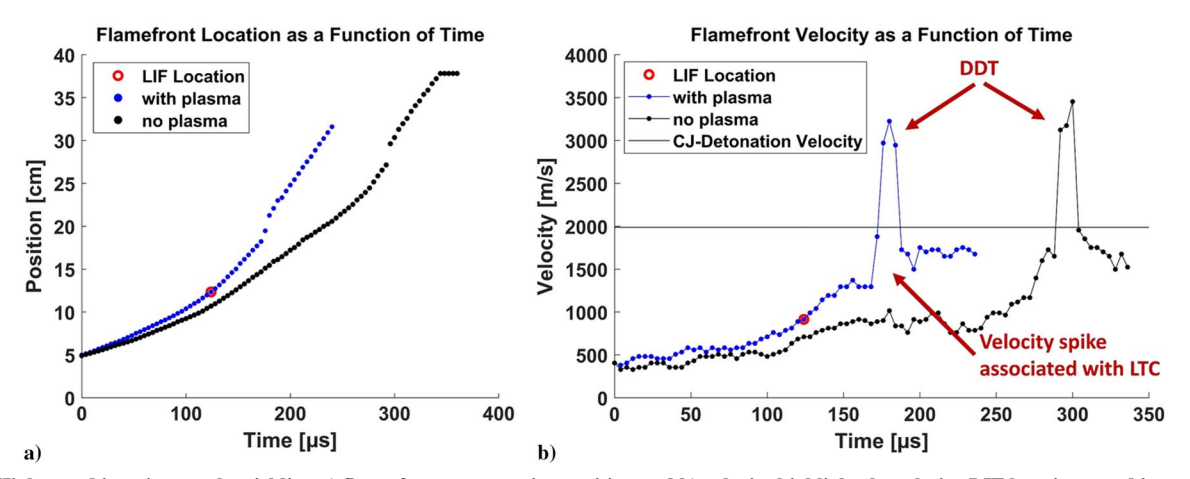


Fig. 2 High-speed imaging results yielding a) flame front propagation position and b) velocity highlight the relative LIF locations used in combustion experiments.

image 5 μ s after the final pulse in each burst is discharged. The LIF signal is acquired at rate of 20 Hz and is synchronized with each burst.

C. Numerical Methods

The calculation of the electric field in the discharge channel is conducted by a multiscale adaptive reduced chemistry solver for plasma-assisted combustion (MARC-PACS) [11-13]. The model incorporates the 2D plasma solver PASSKEy [14,15] and the adaptive simulation of unsteady reactive flow solver ASURF+ [16,17]. The drift-diffusion-reaction equations for plasma species, Helmholtz equations for photoionization, Poisson equation for electric field, energy conservation equations for plasma discharge and electrons, as well as unsteady, multicomponent, reactive, compressible Navier-Stokes (N-S) equations are solved by time-splitting solution methods. A detailed description for governing equations and numerical schemes can be found in [11,13]. In this work, the calculation is simplified as a one-dimensional (1D) problem as it is assumed that plasma discharge is uniform parallel to the discharge channel. The discharge gap is 1 mm and the thickness of Kapton dielectric layer is ~0.089 mm. The relative dielectric constant of Kapton is 3.4. The mesh size in the computation domain is 1 μ m.

To understand CH₂O production in the plasma-assisted DME/O₂/Ar discharge, the time evolutions of CH₂O and plasmaassisted ignition are calculated by a zero-dimensional (0D) hybrid ZDPlasKin-CHEMKIN model [18–20]. The model incorporates the plasma kinetics solver ZDPlasKin [21] and the combustion kinetics solver by CHEMKIN [22] by a time-splitting scheme. The electron impact rate constants are calculated by the Boltzmann equation solver BOLSIG+ [23], which incorporates in ZDPlasKin [21]. A plasma-assisted DME/ O_2 /Ar combustion kinetic model is developed based on [24]. The model consists of a plasma kinetic submodel and a combustion kinetic submodel. The plasma kinetic submodel incorporates the reactions of electronically excited species $O_2(a^1\Delta_g), O_2(b^1\Sigma_g^+), O_2^*, O(^1D), O(^1S), Ar^*, Ar_2; ions\ CH_3OCH_3^+$ $O_2^+, O_4^+, Ar^+, Ar_2^+, O^-, O_2^-, O_4^-$; and electron. The vibrationally excited species CH₃OCH₃(v = 1-5) and O₂(v = 1-4) are considered to provide gas heating by fast vibrational-translational relaxation. A DME combustion mechanism validated recently at high pressures from Wang et al. [25] is used for the combustion submodel.

The experimentally measured voltage waveform is used as input for numerical modeling. The calculation for plasma discharge is conducted at atmospheric pressure and an initial temperature of 293 K. The detailed kinetic mechanisms can be found in Supplementary Materials.

D. Electric-Field-Induced Second Harmonic Generation

Electric-field-induced second harmonic generation (E-FISH) is conducted within the channel in order to characterize the electric field strength of the plasma ahead of breakdown for comparison with



Fig. 3 Schematic diagram showing top-down view of femtosecond (fs) beam entering the cell for E-FISH.

the model. The details of E-FISH techniques are substantially documented and will not be covered here [26,27]. To probe the electric field in a microchannel plasma, which is immediately adjacent to the two quartz windows, a 1 kHz, 785 nm, femtosecond (fs) laser is chirped to 1 ps with a grating stretcher to prevent higher-order mixing and white light generation in windows near the beam focal point. To effectively distance the focal point from the windows, the beam enters the channel at 5° ; this geometry is shown in Fig. 3. The incident beam is $625~\mu J$, with $\sim 268~\mu J$ entering the plasma region.

III. Results and Analysis

In the experimental study, a fixed quantity of discharge pulses, 500, is applied before ignition to observe the plasma enhancement of LTC via CH₂O measurements. The CH₂O formation in the region associated with plasma-enhanced DME low-temperature oxidation is examined, and the characteristic resultant images are shown in Fig. 4. In Fig. 4a, a case without plasma discharge, we see strong chemiluminescence in the flame zone and only a weak CH₂O LIF signal near the flame front in this region. This is reasonable because, near the flame front, CH2O is formed as an intermediate species in the preheating zone via CH₃O + OH/O reactions. In Fig. 4b, with plasma, we instead see a very strong CH₂O LIF signal in a broad plasma region ahead of the flame front spanning nearly 2 cm. This region of the flow is a shock precompression zone, suggesting that there is a coupling between plasma-enhanced LTC and the shock preheating [10]. The observed CH₂O concentration increase via reaction (1) is a clear indication of plasma-enhanced LTC [28,29] and its impact on the process of low-temperature fuel oxidation. Therefore, the present experiments not only show that a nanosecond discharge can accelerate LTC of DME in a microchannel but also accelerates the detonation transition via the coupling of shock compression and plasma-enhanced LTC.

$$CH2OCH2O2H = 2CH2O + OH$$
 (1)

Figure 5 shows the electric field in the discharge gap by both E-FISH measurements and 1D numerical modeling. The time evolution of electric field is obtained at the center of the discharge gap. The numerical modeling agrees with the E-FISH measurements during the voltage rise and in the maximum electric field strength. However, in the model prediction, the breakdown occurs much more quickly than in the experimental E-FISH measurement. In numerical modeling, the sheath formation near the electrode inhibits the energy

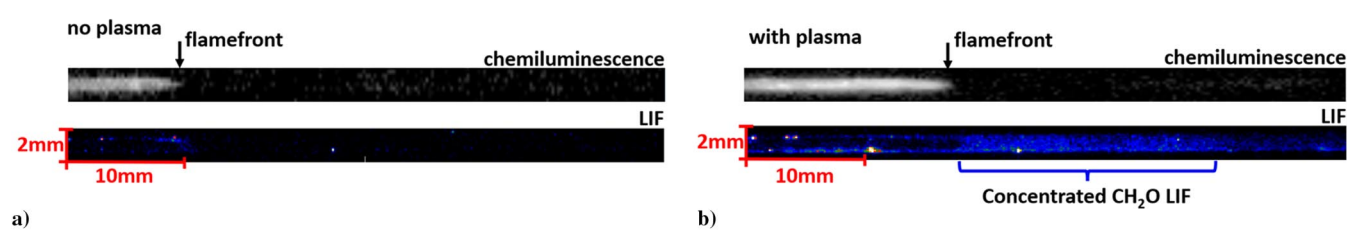


Fig. 4 Chemiluminescence and corresponding CH₂O LIF images for combustion experiments for cases both a) without and b) with plasma applied before ignition.

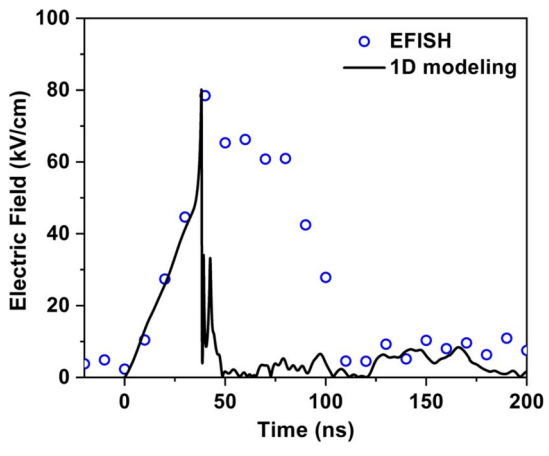


Fig. 5 E-FISH measurement in cell showing field strength from applied plasma with numerical modeling results.

coupling to the discharge channel after breakdown. Therefore, the electric field in the center of the discharge gap is reduced. The kink (the lower electric field peaks after the first one) of the electric field during the breakdown caused during the rapid sheath motion to its quasi-steady-state location near the wall [30]. The difference between experiment and modeling may be caused by the alignment of the laser. Likely, the laser is off center in this narrow channel and is measuring the field within the sheath.

To understand the effects of plasma pulses on the acceleration of detonation transition and CH_2O formation, the time evolutions of electrons, excited species, and radicals in a nanosecond discharge pulse by 0D modeling are presented in Fig. 6. The calculation is conducted with a constant temperature of 293 K due to the minor temperature change in the experiment. The gray region indicates the 200 ns discharge, and the white region indicates the afterglow stage. In the discharge region, the electrons increase first due to electron impact ionization. The electronically excited $O(^1D)$, O_2^* , and Ar^*

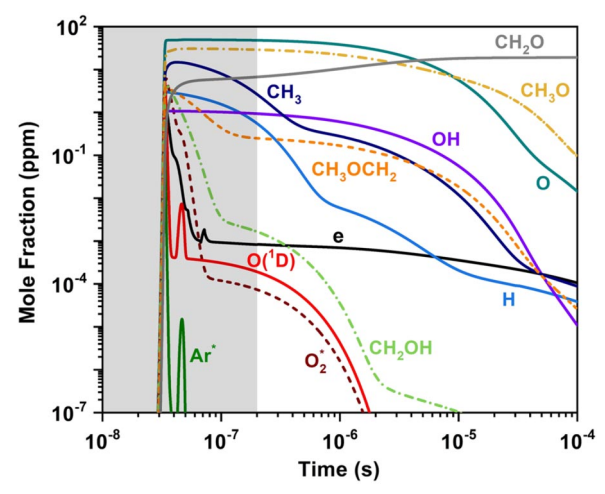


Fig. 6 Time evolutions of electronically excited species, radicals, and electrons in a discharge pulse and afterglow stage.

concentrations increase by electron impact reactions (2–4). The quenching reaction of Ar^* (5) also promotes the production of $O(^1D)$.

$$e + O_2 \rightarrow e + O + O(^1D)$$
 (2)

$$e + O_2 \rightarrow e + O_2^* \tag{3}$$

$$e + Ar \rightarrow e + Ar^*$$
 (4)

$$Ar^* + O_2 \rightarrow Ar + O + O(^1D)$$
 (5)

Figure 6 shows that the radicals O and CH₃O have the highest concentration in the discharge. O is primarily produced by electron impact dissociation reactions (2) and (6) as well as quenching of O(1 D) through reaction (7). The DME dissociation by O(1 D), O₂* and electrons, contributes to CH₃O and other radical production via reactions (8–11) at room temperature. The radicals produced by plasma further accelerate the fuel oxidation through LTC RO₂ (R is the fuel radical) chain-branching and chain-propagation reactions [28,29], which will be discussed later.

$$e + O_2 \rightarrow e + O + O \tag{6}$$

$$O(^{1}D) + O_{2} \rightarrow O + O_{2}(b^{1}\Sigma_{g}^{+})$$
 (7)

$$O(^{1}D) + CH_{3}OCH_{3} \rightarrow CH_{2}OH + CH_{3}O$$
 (8)

$$O(^{1}D) + CH_{3}OCH_{3} \rightarrow CH_{3}O + CH_{3}O$$
 (9)

$$O_2^* + CH_3OCH_3 \rightarrow O_2 + CH_3O + CH_3$$
 (10)

$$e + CH3OCH3 \rightarrow e + CH3O + CH3$$
 (11)

It is noted that the concentrations of electrons and electronically excited species decrease after 40 ns, which is still in the discharge region. This is due to the sheath shielding after the occurrence of breakdown. This results in the termination of ionization and energy deposition to the plasma, which is also observed in modeling results of electric field strength in Fig. 5. Therefore, the production of electrons and electronically excited species is terminated. It is seen that the CH₂O concentration increases in the afterglow stage. This is due to the CH₂OH generated by plasma further accelerating the CH₂O production during the discharge pulses.

Figure 7 shows that the ignition delay time comparison as a function of temperature between autoignition without plasma discharge and plasma-assisted ignition with 500 prepulses by 0D modeling. The two-stage ignition is observed at the autoignition case below 860 K. The ignition delay time is defined as the time interval between the starting point and the maximum rate of temperature rise of the first-stage and second-stage ignitions. The negative temperature coefficient (NTC) region at which the ignition delay time increases with temperature is also observed due to competition between chain-branching and chain-termination reactions in LTC. With 500 prepulses, it is clear to see that the ignition delay time decreases significantly at both first- and second-stage ignitions. The NTC region disappears compared to autoignition. This is due to the chemically active species, such as electrons, electronically excited

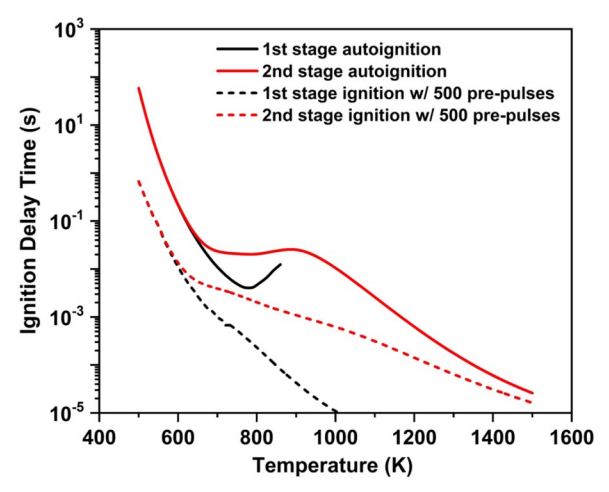


Fig. 7 Ignition delay comparison of autoignition and plasma-assisted ignition with 500 prepulses.

 $O(^1D)$, O_2^* , and Ar^* , as well as radicals, generated by plasma accelerating the fuel oxidation at low temperatures. Figure 7 shows that the first-stage ignition still exists above 860 K in plasma-assisted ignition. This rapid temperature rise is caused by fast heat release from the reactions of the radicals produced by plasma.

To address the enhancement of plasma on LTC, the reaction rate of $CH_2OCH_2O_2H = 2CH_2O + OH$ and temperature of autoignition and plasma-assisted ignition with 500 prepulses are compared with an initial temperature of 600 K, as shown in Fig. 8. The results clearly show that the rate of reaction (1) is several orders of magnitude higher with 500 plasma prepulses compared with autoignition at 600 K, indicating the acceleration of LTC by plasma. Due to the efficient production of O through electron impact dissociation on O2 via reactions (2) and (6), the CH₃OCH₂ and OH are formed by the H-abstraction reaction (12). The OH production further accelerates DME consumption and CH₃OCH₂ production by reaction (13). CH₃OCH₂O₂ is produced by an addition reaction (14) of CH₃OCH₂ and O2. The isomerization of CH3OCH2O2 produces CH2OCH2O2H through reaction (15). Then, the decomposition of CH₂OCH₂O₂H contributes to the production of CH₂O and OH via reaction (1). At the same time, the CH₂OCH₂O₂H can also produce peroxy hydroperoxyl alkyl radical O₂CH₂OCH₂O₂H by an addition reaction with O₂ (16). The O₂CH₂OCH₂O₂H promotes the OH production by decomposition via reactions (17) and (18).

$$CH3OCH3 + O = CH3OCH2 + OH$$
 (12)

$$CH3OCH3 + OH = CH3OCH2 + H2O$$
 (13)

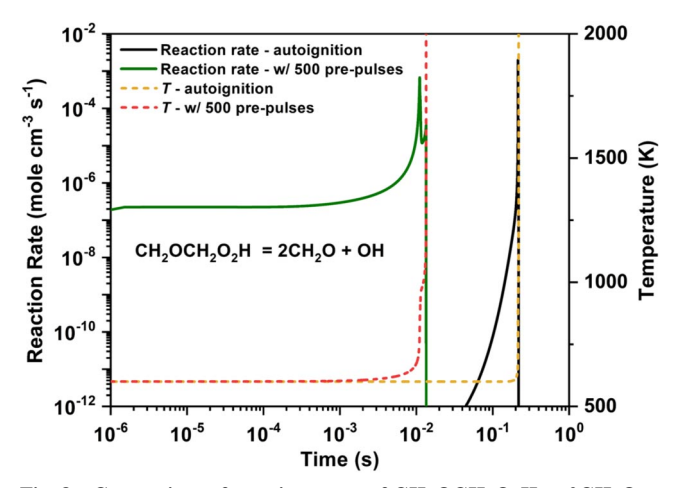


Fig. 8 Comparison of reaction rate t of $CH_2OCH_2O_2H = 2CH_2O + OH$ and temperature of autoignition and plasma-assisted ignition with 500 prepulses at 600 K.

$$CH3OCH2 + O2 = CH3OCH2O2$$
 (14)

$$CH3OCH2O2 = CH2OCH2O2H (15)$$

$$CH_2OCH_2O_2H + O_2 = O_2CH_2OCH_2O_2H$$
 (16)

$$O_2CH_2OCH_2O_2H = HO_2CH_2OCHO + OH$$
 (17)

$$HO_2CH_2OCHO = OCH_2OCHO + OH$$
 (18)

From the above discussion, we can conclude that plasma can significantly accelerate the DME low-temperature oxidation and enhance ignition and ignition—shock coupling. This ignition enhancement further accelerates the detonation transition, as shown in Fig. 2.

To address the question of the delayed DDT onset with a large number of plasma pulses, now knowing that the plasma enhances the LTC, further experimentation and numerical simulation are carried out. Single bursts of 10, 50, and 100 ns-DBD pulses (pulse width 200 ns, peak voltage 10 kV, pulse repetition rate 10 kHz) are applied at 20 Hz across the detonation channel. Each burst is in synchronization with the Nd: YAG laser. With each discharge, CH₂O is generated in the channel and is observed with LIF. The resulting formaldehyde LIF signal intensity and simulated mole fractions as a function of time for each of the different burst conditions are plotted in Fig. 9. The heat loss coefficient is considered in the calculation due to temperature rise with different discharge pulses burst. From the LIF intensity, we observe that the CH₂O concentration increases before 0.7 s, regardless of the burst size and, hence, total premixture preparation time. It is also shown that the number of discharges per burst affects the peak CH₂O concentration. Figure 9 shows that the peak formaldehyde concentration grows with burst size. This increase is associated with the increase of the total discharge energy spent for the mixture excitation. The 10-times increase in energy from 10 to 100 pulses per burst leads to 5-times increase in peak formaldehyde LIF intensity due to the increase of radical production rate. After ~1 s, the LIF intensity at the 50- and 100-pulse burst decreases with more discharge pulses applied. This is because the partial fuel oxidation leads to the decrease of CH₂O production and the increase of CH₂O consumption by OH and O after the fuel is used up, which will be discussed later. Compared with the LIF measurement, the numerical modeling by including wall heat loss in Fig. 9 shows the same tendency with different plasma bursts. However, the model fails to predict the timing of peak CH₂O concentration with 50-pulse burst as well as the decreasing of CH₂O. This may be for two reasons. First, the prediction of heat loss in the present 0D model may cause the deviation from the experiment. Second, the reactions between electrons and intermediate species such as CH₃OCH₂ and CH₂OH not

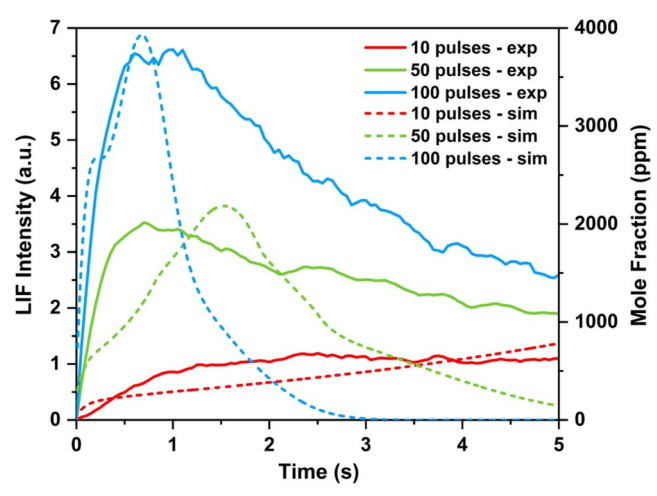


Fig. 9 Time evolutions of CH_2O LIF intensity by experiment and mole fraction by numerical modeling with different ns-DBD pulses at a fixed burst period and rate. (The CH_2O mole fraction by numerical modeling is plotted every 50 ms, which is consistent with the LIF measurement.)

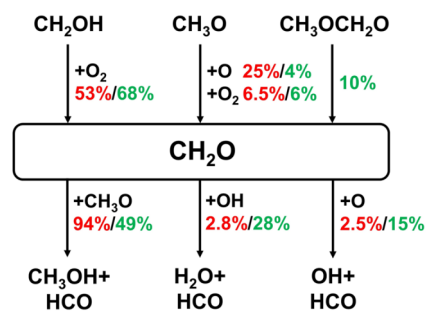


Fig. 10 Production and consumption pathways of CH_2O with a) 10-pulse (red) and b) 100-pulse burst (green). All percentages do not sum to 100%, as some reactions add small quantities. The percentages indicate the contributions accounting for the total CH2O production and consumption.

considered in the present plasma model also contribute to $\mathrm{CH}_2\mathrm{O}$ production.

To understand the production and consumption pathways of CH_2O with different plasma bursts, the path flux analysis with different pulse-bursts is conducted by numerical modeling, as shown in Fig. 10. Figure 9 shows that the mole faction of CH_2O increases with more discharge pulses when the pulse-burst is 10. This is because the DME is partially oxidized in the plasma discharge with fewer pulse numbers. The consumption of CH_2O is less than the production path flux. The electronically excited $O(^1D)$ and O_2^* as well as electrons contribute to the production of CH_2OH and CH_3O through reactions (8–11). At the 10-pulse burst condition, CH_2OH is the major species accelerating the CH_2O production via reaction (19). The production of CH_3O also contributes to CH_2O production via reactions (20) and (21). However, the consumption of CH_2O by CH_3O through reaction (22) plays a more dominant role compared with the production pathways (20) and (21).

$$CH_2OH + O_2 = CH_2O + HO_2$$
 (19)

$$CH_3O + O = CH_2O + OH (20)$$

$$CH_3O + O_2 = CH_2O + HO_2$$
 (21)

$$CH2O + CH3O = HCO + CH3OH (22)$$

With the increase of pulse burst (above 50-pulse burst), Fig. 9 shows that the CH_2O mole faction firstly increases and then decreases with more pulses. With 100-pulse burst 43% of CH_2O is consumed by the reactions with OH and O though reactions (23) and (24), as shown in Fig. 10.

$$CH2O + OH = HCO + H2O (23)$$

$$CH2O + O = HCO + OH$$
 (24)

After the fuel is used up, $\mathrm{CH}_2\mathrm{O}$ is gradually consumed by OH and O with more discharge pulses. This leads to the reduction of heat release and therefore the delay of DDT.

IV. Conclusions

Plasma-enhanced LTC effect on DDT in a microchannel with ns-DBD experiments has been carried out at atmospheric pressure in a fuel-lean DME/ O_2 /Ar mixture. The results show that transversal ns-DBD can chemically sensitize the LTC of the mixture. Formaldehyde produced via plasma-enhanced LTC is most concentrated in the region immediately ahead of the propagating flame front. The plasma-enhanced LTC together with adiabatic compression waves enhances the coupling between ignition and shock wave and thus leads to faster DDT. The present study not only demonstrates the ability of ns-DBD plasma to accelerate the LTC of DME in a microchannel, but also demonstrates that the enhanced LTC is coupled with

the shock compression. It is this coupling that can then be used to control DDT development and onset of the detonation spatially and temporally. This is the first example of measured CH_2O distribution to demonstrate plasma-assisted DDT via kinetic enhancement of LTC.

In addition to demonstrating that the enhanced LTC can be used to control detonation onset, additional insight into how the DDT affected by ns-DBD is gained through examination of the formaldehyde concentration growth and decay over time with consistent bursts of the discharge. The competition between the kinetic enhancement of ignition and the reduction of heat release rate is observed for different pulse conditions, and a consistent optimal cumulative pulse count is observed. The observed disparity in peak concentrations suggests that there is an optimal timing for pre-ignition discharges to best leverage the LTC enhancement to accelerate DDT and the detonation onset.

The simulated time evolutions of species show that the electronically excited species $(O(^1D), O_2^*$ and $Ar^*)$ and electrons generated in the plasma discharge promote the radical and CH₂O production. The results show that the ignition delay time is significantly shortened and NTC region disappears with 500 plasma prepulses by accelerating the low-temperature fuel oxidation. The O radicals produced by plasma promote the production of OH and CH₃OCH₂, which further accelerates the CH₂O and OH production via CH₃OCH₂ + $O_2 \rightarrow CH_3OCH_2O_2 \rightarrow CH_2OCH_2O_2H \rightarrow 2CH_2O + OH$. Meanwhile, the production of CH₂OCH₂O₂H also promotes the production of OH and therefore DME oxidation via $CH_2OCH_2O_2H + O_2 \rightarrow O_2$ $CH_2OCH_2O_2H \rightarrow HO_2CH_2OCHO + OH \rightarrow OCH_2OCHO + 2OH.$ This further accelerates the DDT. The CH₂O concentration with different plasma burst shows that CH2O is consumed by OH and O radicals after the DME is used up. This indicates that the delay of deflagration to detonation is caused by the heat release reduction from fuel oxidation with more discharge pulses.

Together, the present work demonstrates that 1) the LTC of DME is enhanced through the application of ns-DBDs, 2) the plasma kinetic enhancement is coupled with the shock compression and preheating generated by the accelerating flame front, and 3) the extent of that enhancement can be controlled by optimizing the balance of radicals and stable intermediates generation and consumption by means of patterned ns-DBD application. The ability to control DDT with plasmas is promising for the development of detonation engines and opens the opportunity to demonstrate further improvement in lean burn flame stability, low-temperature fuel oxidation and processing, as well as emission reduction.

Acknowledgments

This material is based upon work supported by the U.S. Department of Energy (DOE) Fusion Energy Sciences (DE-SC0020233, DE-SC0021217), National Nuclear Security Administration (DE-NA0003525), the NSF grant CBET 1903362, and Office of Science Graduate Student Research (SCGSR) program. The SCGSR program is administered by the Oak Ridge Institute for Science and Education for the DOE. Christopher Kliewer and Scott Steinmetz: This material is based upon work supported by the U.S. Department of Energy, Office of Science, Office of Fusion Energy Sciences under contract number DE-NA0003525. This research used resources of the Low Temperature Plasma Research Facility at Sandia National Laboratories, which is a collaborative research facility supported by the U.S. Department of Energy, Office of Science, Office of Fusion Energy Sciences. The views expressed in this paper do not necessarily represent the views of the U.S. Department of Energy or the United States Government.

References

- [1] Schwer, D. A., and Kailasanath, K., "Rotating Detonation-Wave Engines," *NRL Review*, 2011, pp. 90–94.
- [2] Journell, C. L., Gejji, R. M., Walters, I. V., Lemcherfi, A. I., Slabaugh, C. D., and Stout, J. B., "High-Speed Diagnostics in a Natural Gas–Air Rotating Detonation Engine," *Journal of Propulsion and Power*, Vol. 36, No. 4, 2020, pp. 498–507. https://doi.org/10.2514/1.B37740

- [3] Stechmann, D. P., Sardeshmukh, S., Heister, S. D., and Mikoshiba, K., "Role of Ignition Delay in Rotating Detonation Engine Performance and Operability," *Journal of Propulsion and Power*, Vol. 35, No. 1, 2019, pp. 125–140. https://doi.org/10.2514/1.B37117
- [4] Ju, Y., and Sun, W., "Plasma Assisted Combustion: Dynamics and Chemistry," *Progress in Energy and Combustion Science*, Vol. 48, June 2015, pp. 21–83. https://doi.org/10.1016/j.pecs.2014.12.002
- [5] Starikovskiy, A., and Aleksandrov, N., "Plasma-Assisted Ignition and Combustion," *Progress in Energy and Combustion Science*, Vol. 39, No. 1, 2013, pp. 61–110. https://doi.org/10.1016/j.pecs.2012.05.003
- [6] Starikovskiy, A., Aleksandrov, N., and Rakitin, A., "Plasma-Assisted Ignition and Deflagration-to-Detonation Transition," *Philosophical Transactions of the Royal Society A: Mathematical, Physical and Engineering Sciences*, Vol. 370, No. 1960, 2012, pp. 740–773. https://doi.org/10.1098/rsta.2011.0344
- [7] Tropina, A. A., and Mahamud, R., "Effect of Plasma on the Deflagration to Detonation Transition," *Combustion Science and Technology*, Vol. 194, No. 13, 2022, pp. 2752–2770. https://doi.org/10.1080/00102202.2021.1888085
- [8] Zhou, S., Wang, F., Che, X., and Nie, W., "Numerical Study of Non-equilibrium Plasma Assisted Detonation Initiation in Detonation Tube," *Physics of Plasmas*, Vol. 12, No. 23, 2016, Paper 123522. https://doi.org/10.1063/1.4972136
- [9] Vorenkamp, M., Steinmetz, S. A., Chen, T. Y., Mao, X., Starikovskiy, A., Kliewer, C., and Ju, Y., "Plasma-Assisted Deflagration to Detonation Transition in a Microchannel with Fast-Frame Imaging and Hybrid fs/ps Coherent Anti-Stokes Raman Scattering Measurements," *Proceedings* of the Combustion Institute, Vol. 39, No. 4, 2023, pp. 5561–5569. https://doi.org/10.1016/j.proci.2022.08.133
- [10] Ssu, H.-W., and Wu, M.-H., "Formation and Characteristics of Composite Reaction—Shock Clusters in Narrow Channels," *Proceedings of the Combustion Institute*, Vol. 38, No. 3, 2021, pp. 3473–3480. https://doi.org/10.1016/j.proci.2020.07.069
- [11] Mao, X., Zhong, H., Zhang, T., Starikovskiy, A., and Ju, Y., "Modeling of the Effects of Non-Equilibrium Excitation and Electrode Geometry on H₂/Air Ignition in a Nanosecond Plasma Discharge," *Combustion* and Flame, Vol. 240, June 2022, Paper 112046.
- https://doi.org/10.1016/j.combustflame.2022.112046
 [12] Mao, X., Zhong, H., Wang, Z., Ombrello, T., and Ju, Y., "Effects of Inter-Pulse Coupling on Nanosecond Pulsed High Frequency Discharge Ignition in a Flowing Mixture," *Proceedings of the Combustion Institute*, Vol. 39, No. 4, 2023, pp. 5457–5464.
 https://doi.org/10.1016/j.proci.2022.06.018
- [13] Chen, T. Y., Mao, X., Zhong, H., Lin, Y., Liu, N., Goldberg, B. M., Ju, Y., and Kolemen, E., "Impact of CH₄ Addition on the Electron Properties and Electric Field Dynamics in a Ar Nanosecond-Pulsed Dielectric Barrier Discharge," *Plasma Sources Science and Technology*, Vol. 31, No. 12, 2022, Paper 125013. https://doi.org/10.1088/1361-6595/acab81
- [14] Zhu, Y., Chen, X., Wu, Y., and Starikovskaia, S., PASSKEy Code [software], http://www.plasmatech.net/parser/passkey/ (Science and Technology of Plasma Dynamics Laboratory, Xi'an, China and Laboratorie de Physique des Plasmas, Paris, France, 2021).
- [15] Zhu, Y., Chen, X., Wu, Y., Hao, J., Ma, X., Lu, P., and Tardiveau, P., "Simulation of Ionization-Wave Discharges: A Direct Comparison Between the Fluid Model and E-FISH Measurements," *Plasma Sources Science and Technology*, Vol. 30, No. 7, 2021, Paper 075025. https://doi.org/10.1088/1361-6595/ac0714
- [16] Sun, W., "Developments of Efficient Numerical Methods for Combustion Modeling with Detailed Chemical Kinetics," Ph.D. Dissertation, Dept. of Mechanical and Aerospace Engineering, Princeton Univ., Princeton, NJ, 2020.
- [17] Chen, Z., Burke, M. P., and Ju, Y., "Effects of Lewis Number and Ignition Energy on the Determination of Laminar Flame Speed Using Propagating Spherical Flames," *Proceedings of the Combustion*

Institute, Vol. 32, No. 1, 2009, pp. 1253–1260. https://doi.org/10.1016/j.proci.2008.05.060

- [18] Mao, X., Rousso, A., Chen, Q., and Ju, Y., "Numerical Modeling of Ignition Enhancement of CH₄/O₂/He Mixtures Using a Hybrid Repetitive Nanosecond and DC Discharge," *Proceedings of the Combustion Institute*, Vol. 37, No. 4, 2019, pp. 5545–5552. https://doi.org/10.1016/j.proci.2018.05.106
- [19] Mao, X., Chen, Q., Rousso, A. C., Chen, T. Y., and Ju, Y., "Effects of Controlled Non-Equilibrium Excitation on H₂/O₂/He Ignition Using a Hybrid Repetitive Nanosecond and DC Discharge," *Combustion and Flame*, Vol. 206, Aug. 2019, pp. 522–535. https://doi.org/10.1016/j.combustflame.2019.05.027
- [20] Zhong, H., Mao, X., Rousso, A. C., Patrick, C. L., Yan, C., Xu, W., Chen, Q., Wysocki, G., and Ju, Y., "Kinetic Study of Plasma-Assisted n-Dodecane/O₂/N₂ Pyrolysis and Oxidation in a Nanosecond-Pulsed Discharge," *Proceedings of the Combustion Institute*, Vol. 38, No. 4, 2021, pp. 6521–6531. https://doi.org/10.1016/j.proci.2020.06.016
- [21] Pancheshnyi, S., Eismann, B., Hagelaar, G. J. M., and Pitchford, L. C., "Computer Code ZDPlasKin," http://www.zdplaskin.laplace.univtlse.fr (University of Toulouse, LAPLACE, CNRS-UPS-INP, Toulouse, France, 2008).
- [22] Kee, R. J., Rupley, F. M., and Miller, J. A., "Chemkin-II: A Fortran Chemical Kinetics Package for the Analysis of Gas-Phase Chemical Kinetics," Sandia National Lab. TR SAND-89-8009, Livermore, CA, 1989.
- [23] Hagelaar, G. J. M., and Pitchford, L. C., "Solving the Boltzmann Equation to Obtain Electron Transport Coefficients and Rate Coefficients for Fluid Models," *Plasma Sources Science and Technology*, Vol. 14, No. 4, 2005, pp. 722–733. https://doi.org/10.1088/0963-0252/14/4/011
- [24] Zhong, H., Yang, X., Mao, X., Shneider, M. N., Adamovich, I. V., and Ju, Y., "Plasma Thermal-Chemical Instability of Low-Temperature Dimethyl Ether Oxidation in a Nanosecond-Pulsed Dielectric Barrier Discharge," *Plasma Sources Science and Technology*, Vol. 31, No. 11, 2022, Paper 114003. https://doi.org/10.1088/1361-6595/ac9a6a
- [25] Wang, Z., Yan, C., Lin, Y., Zhou, M., Jiang, B., Liu, N., Zhong, H., and Ju, Y., "Kinetics and Extinction of Non-Premixed Cool and Warm Flames of Dimethyl Ether at Elevated Pressure," *Proceedings of the Combustion Institute*, Vol. 39, No. 2, 2023, pp. 1871–1879. https://doi.org/10.1016/j.proci.2022.06.007
- [26] Raskar, S., Orr, K., Adamovich, I. V., Chng, T. L., and Starikovskaia, S. M., "Spatially Enhanced Electric Field Induced Second Harmonic (SEEFISH) Generation for Measurements of Electric Field Distributions in High-Pressure Plasmas," *Plasma Sources Science and Technology*, Vol. 31, No. 8, 2022, Paper 085002. https://doi.org/10.1088/1361-6595/ac8072
- [27] Dogariu, A., Goldberg, B. M., O'Byrne, S., and Miles, R. B., "Species-Independent Femtosecond Localized Electric Field Measurement," *Physical Review Applied*, Vol. 7, No. 2, 2017, Paper 024024. https://doi.org/10.1103/PhysRevApplied.7.024024
- [28] Ju, Y., "Understanding Cool Flames and Warm Flames," Proceedings of the Combustion Institute, Vol. 38, Jan. 2021, pp. 83–119. https://doi.org/10.1016/j.proci.2020.09.019
- [29] Ju, Y., Reuter, C. B., Yehia, O. R., Farouk, T. I., and Won, S. H., "Dynamics of Cool Flames," *Progress in Energy and Combustion Science*, Vol. 75, Nov. 2019, Paper 100787. https://doi.org/10.1016/j.pecs.2019.100787
- [30] Adamovich, I. V., Nishihara, M., Choi, I., Uddi, M., and Lempert, W. R., "Energy Coupling to the Plasma in Repetitive Nanosecond Pulse Discharges," *Physics of Plasmas*, Vol. 16, Nov. 2009, Paper 113505. https://doi.org/10.1063/1.3264740

L. Qiao Associate Editor